A&A 429, 417–426 (2005)
DOI: 10.1051/0004-6361:20048093
© ESO 2004

Astronomy & Astrophysics

The selection function of SZ cluster surveys

J.-B. Melin, J. G. Bartlett, and J. Delabrouille

APC – Université Paris 7, 75005 Paris, France
PCC – Collège de France, 75005 Paris, France
e-mail: [melin;bartlett;delabrouille]@cdf.in2p3.fr

Received 15 April 2004 / Accepted 11 September 2004

Abstract. We study the nature of cluster selection in Sunyaev-Zel'dovich (SZ) surveys, focusing on single frequency observations and using Monte Carlo simulations incorporating instrumental effects, primary cosmic microwave background (CMB) anisotropies and extragalactic point sources. Clusters are extracted from simulated maps with an optimal, multi-scale matched filter. We introduce a general definition for the survey selection function that provides a useful link between an observational catalog and theoretical predictions. The selection function defined over the observed quantities of flux and angular size is independent of cluster physics and cosmology, and thus provides a useful characterization of a survey. Selection expressed in terms of cluster mass and redshift, on the other hand, depends on both cosmology and cluster physics. We demonstrate that SZ catalogs are not simply flux limited, and illustrate how incorrect modeling of the selection function leads to biased estimates of cosmological parameters. The fact that SZ catalogs are not flux limited complicates survey "calibration" by requiring more detailed information on the relation between cluster observables and cluster mass.

Key words. cosmology: large-scale structure of Universe – galaxies: clusters: general

1. Introduction

Galaxy cluster surveys are important tools for measuring key cosmological quantities and for understanding the process of structure formation in the universe (Bahcall et al. 1999; Rosati et al. 2002). Surveying for clusters using the Sunyaev-Zel'dovich (SZ) effect (Sunyaev & Zeldovich 1970; Sunyaev & Zeldovich 1972; for recent reviews, see Birkinshaw 1999; and Carlstrom et al. 2002) offers a number of advantages over more traditional methods based on X-ray or optical imaging. These advantages include good detection efficiency at high-redshift; a selection based on the thermal energy of the intracluster medium, a robust quantity relative to any thermal structure in the gas; and an almost constant mass detection limit with redshift (Holder et al. 2000; Bartlett 2000; Bartlett 2001). A new generation of optimized, dedicated instruments, both large bolometer arrays (Masi et al. 2003; Runyan et al. 2003; Kosowsky 2004) and interferometers (Lo et al. 2000; Jones 2002), will soon perform such SZ cluster surveys, and we may look forward to the large and essentially full-sky SZ catalog expected from the Planck mission[1]. In anticipation, many authors have studied the nature and use of SZ cluster catalogs and made predictions for the number of objects expected from various proposed surveys (Holder et al. 2000; Kneissl et al. 2001). A good example of the potential of an SZ survey is the use of its redshift distribution to examine structure formation at high redshift and to thereby constrain cosmological parameters, such as the density parameter $\Omega_{\rm M}$ (Barbosa et al. 1996), and the dark energy equation-of-state ω (Haiman et al. 2001).

An astronomical survey is fundamentally characterized by its selection function, which identifies the subclass of objects detected among all those actually present in the survey area. It is a function of cluster properties and survey conditions. Depending on the nature of the observations, relevant cluster properties may include: mass, redshift, luminosity, morphology, etc., while key descriptors of the survey would be sensitivity, angular resolution, spectral coverage, etc. The selection function will also depend on the the detection algorithm used to find clusters in the survey data. Understanding of the selection function is a prerequisite to any statistical application of the survey catalog; otherwise, one has no idea how representative the catalog is of the parent population actually out in the universe.

Selection function issues for SZ surveys have been touched on recently by several authors (Bartlett 2001; Schulz & White 2003; White 2003), while most previous studies of the potential use of SZ surveys have not examined this point in detail. For example, predictions of the redshift distribution of SZ-detected clusters usually assume that they are point sources, simply selected on their total flux[2]. We shall see below that this is not necessarily the case, and an analysis of cosmological

[1] A list of web pages describing a number of experiments is given in the reference section.

[2] The term *flux* does not really apply in the case of SZ observations, as the effect is measured relative to the unperturbed background and may be negative. We shall nevertheless use it throughout for simplicity.

Article published by EDP Sciences and available at http://www.aanda.org or http://dx.doi.org/10.1051/0004-6361:20048093

parameters based on such an assumption would significantly bias the results.

Understanding a survey selection function is difficult. By its very nature and purpose, the selection function is supposed to tell us about objects that we *don't see* in the survey! Realistic simulations of a survey are central to determining its selection function (e.g., Adami et al. 2001). One knows which objects are put into the simulation and can then compare them to the subset of objects detected by the mock observations. In practice, of course, understanding of a selection function comes only from a combination of such simulations and diverse observations taken under different conditions and/or in different wavebands; full understanding thus comes slowly.

There are really two distinct issues connected to the selection function: object detection, or *survey completeness*, and object measurement, which we shall refer to as *photometry*; as a separate issue, one must also determine the contamination function. One would like to characterize each detected cluster by determining, for example, its total flux, angular size, etc. As practitioners are well aware, photometry of extended objects faces many difficulties that introduce additional uncertainty and, in particular, potential bias into the survey catalog. The selection function must correct for bias induced by both the detection and photometric procedures. The two are, however, distinct steps in catalog construction, and the selection function (see below) should reflect this fact.

The object of the present work is to begin a study of SZ selection functions for the host of SZ surveys that are being planned, and to propose a formalism for their characterization. To this end, we have developed a rapid Monte Carlo simulation tool (Delabrouille et al. 2002) that produces mock images of the SZ sky, including various clustering and velocity effects, primary cosmic microwave background (CMB) anisotropies, radio point sources and instrumental effects. The main goals of such studies, in this period before actual surveying has begun, are to improve understanding of the expected scientific return of a given survey and to help optimize observing strategies.

Our specific aim in the present work is to study selection effects in SZ surveys by focusing on single frequency observations, such as will be performed by up-coming interferometers. Most bolometer cameras propose surveys at several frequencies, although not necessarily simultaneously; the present considerations are therefore applicable to the first data sets from these instruments. This work builds on that of Bartlett (2000) by adding the effects of primary CMB anisotropies, point sources and photometric errors, and by the use of an optimized cluster detection algorithm (Melin et al. 2004).

General considerations concerning the selection function are given in the next section and used to motivate our definition given in Eq. (1). We then briefly describe (Sect. 3) our simulations, based on a Monte Carlo approach incorporating cluster correlations and velocities, as well as our cluster detection and photometry algorithms built on an optimized spatial filter (details will be given elsewhere, Melin et al. 2004). A discussion of cluster selection with this method follows (Sect. 4), where with a simple analytic argument, we show how cluster detection depends on *both* total flux and angular size. Our main conclusion is that SZ surveys will not be simply flux limited. Our simulations support the analytical expectations, and they also highlight the difficulty of performing accurate photometry on detected clusters.

We close with a discussion (Sect. 5) of some implications for upcoming surveys. The most important is that the redshift distribution of observed clusters differs from that of a pure flux-limited catalog; assuming pure flux selection will therefore lead to biased estimates of cosmological parameters. In this same section, we give an explicit example of biased parameter estimation caused by the presence of incorrectly modeled excess primary CMB power on cluster scales, as suggested by the CBI experiment (Mason et al. 2001). We note that non-trivial cluster selection complicates survey "calibration" (Bartelmann 2001; Hu 2003; Majumdar & Mohr 2003; Lima & Hu 2004) because a *size-mass* relation must be obtained in addition to a *flux-mass* relation. Photometric errors will further increase the difficulty by augmenting scatter in the mass-observable relations.

2. Selection function: General considerations

To motivate our definition, we first consider some general properties desired of a survey selection function. Fundamentally, it relates observed catalog properties (e.g., flux and size) to relevant intrinsic characteristics of the source population under study. In particular, we want it to tell us about the *completeness* of the survey catalog as a function of source properties, which is a measure of the selection bias. In addition, we also wish for it to reflect the effects of statistical (e.g., photometric) errors. Notice, on the other hand, that the selection function will not tell us anything about *contamination* of the catalog by false detections; this is another function of observed quantities that must be separately evaluated.

Consider the example of a flux-limited catalog of point sources. Neglecting photometric measurement errors, the probability that a source at redshift z will find its way into the survey catalog is simply given by the fraction of sources brighter than the flux limit, which may be calculated as an integral over the luminosity function at z (e.g., Peebles 1993). Extended objects complicate the situation, for their detection will in general depend on morphology. One must then define appropriate source descriptors other than just a total flux; and even the definition of total flux, conceptually simple, becomes problematic (fixed aperture flux, isophotal flux, integrated flux with a fitted profile, etc.). The choice of descriptors is clearly important and the selection function will depend on it. They must encode relevant observational information on the sources and represent observables with as little measurement error as possible.

The simplest characterization for extended SZ sources would employ a total observed flux, $Y_{\rm o}$, and a representative angular size, which we take to be the core radius $\theta_{\rm co}$. By total flux, we mean the flux density integrated over the entire cluster profile, out to the virial radius, and we express it in a frequency independent manner as the integrated Compton-y parameter. We limit ourselves to these two descriptors in the ensuing discussion, although clearly many others describing cluster morphology are of course possible (ellipticity, for example...). How the observed quantities are actually measured is crucial –

measurement errors and the selection function will both depend on the technique used.

Our detected clusters will then populate the observed parameter space according to some distribution $\mathrm{d}N_\mathrm{o}/\mathrm{d}Y_\mathrm{o}\mathrm{d}\theta_\mathrm{co}$. What we really seek, however, is the true cluster distribution, $\mathrm{d}N/\mathrm{d}Y\mathrm{d}\theta_\mathrm{c}$, over the intrinsic cluster parameters Y and θ_c. Measurement errors and catalog incompleteness both contribute to the difference between these two distributions. In addition, the catalog will suffer from contamination by false detections.

These general considerations motivate us to define the *selection function* as the *joint distribution of* Y_o *and* θ_co, as a function of (i.e., given) Y and θ_c. There are many other factors that influence the selection function, such as instrument characteristics, observation conditions and analysis methods, so in general we write

$$\Phi\left[Y_\mathrm{o}, \theta_\mathrm{co}|Y, \theta_\mathrm{c}, \sigma_\mathrm{N}, \theta_\mathrm{fwhm}, ...\right] \tag{1}$$

where θ_fwhm is the *FWHM* of an assumed Gaussian beam and σ_N^2 is the map noise variance. We illustrate our main points throughout this discussion with simple uniform Gaussian white noise. The dots represent other possible influences on the selection function, such as the detection and photometry algorithms employed to construct the catalog.

Several useful properties follow from this definition. For example, the selection function relates the observed counts from a survey to their theoretical value by

$$\frac{\mathrm{d}N_\mathrm{o}}{\mathrm{d}Y_\mathrm{o}\mathrm{d}\theta_\mathrm{co}}(Y_\mathrm{o}, \theta_\mathrm{co}) = \int_0^\infty \mathrm{d}Y \int_0^\infty \mathrm{d}\theta_\mathrm{c}\ \Phi(Y_\mathrm{o}, \theta_\mathrm{co}|Y, \theta_\mathrm{c}) \times \frac{\mathrm{d}N}{\mathrm{d}Y\mathrm{d}\theta_\mathrm{c}}(Y, \theta_\mathrm{c})\,. \tag{2}$$

A similar relation can be established between the observed counts and cluster mass and redshift:

$$\frac{\mathrm{d}N_\mathrm{o}}{\mathrm{d}Y_\mathrm{o}\mathrm{d}\theta_\mathrm{co}}(Y_\mathrm{o}, \theta_\mathrm{co}) = \int_0^\infty \mathrm{d}z \int_0^\infty \mathrm{d}M\ \Psi(Y_\mathrm{o}, \theta_\mathrm{co}|z, M) \times \frac{\mathrm{d}N}{\mathrm{d}z\mathrm{d}M}(z, M) \tag{3}$$

where $\mathrm{d}N/\mathrm{d}z\mathrm{d}M$ is the mass function and Ψ incorporates the intrinsic and observational scatter in the relation between $(Y_\mathrm{o}, \theta_\mathrm{co})$ and (z, M) (mass-observable relations). This is made more explicit by

$$\Psi(Y_\mathrm{o}, \theta_\mathrm{co}|z, M) = \int_0^\infty \mathrm{d}Y \int_0^\infty \mathrm{d}\theta_\mathrm{c}\Phi(Y_\mathrm{o}, \theta_\mathrm{co}|Y, \theta_\mathrm{c}) \times T(Y, \theta_\mathrm{c}|z, M) \tag{4}$$

where the function T represents the intrinsic scatter in the relation between actual flux Y and core radius θ_c, and cluster mass and redshift.

In general, we may separate the selection function into two parts, one related to detection and the other to photometry:

$$\Phi(Y_\mathrm{o}, \theta_\mathrm{co}|Y, \theta_\mathrm{c}) = \chi(Y, \theta_\mathrm{c})F(Y_\mathrm{o}, \theta_\mathrm{co}|Y, \theta_\mathrm{c}). \tag{5}$$

The first factor represents survey completeness and is simply the ratio of detected to actual clusters as a function of true cluster parameters. The second factor quantifies photometric errors with a distribution function F normalized to unity:

$$\int \mathrm{d}Y_\mathrm{o}\mathrm{d}\theta_\mathrm{co}\ F(Y_\mathrm{o}, \theta_\mathrm{co}|Y, \theta_\mathrm{c}) = 1$$

In the absence of measurement errors we would have

$$\Phi(Y_\mathrm{o}, \theta_\mathrm{co}|Y, \theta_\mathrm{c}) = \chi(Y_\mathrm{o}, \theta_\mathrm{co})\delta(Y_\mathrm{o} - Y)\delta(\theta_\mathrm{co} - \theta_\mathrm{c})$$

in which case the observed counts become

$$\frac{\mathrm{d}N_\mathrm{o}}{\mathrm{d}Y_\mathrm{o}\mathrm{d}\theta_\mathrm{co}}(Y_\mathrm{o}, \theta_\mathrm{co}) = \chi(Y_\mathrm{o}, \theta_\mathrm{co})\frac{\mathrm{d}N}{\mathrm{d}Y\mathrm{d}\theta_\mathrm{c}}(Y, \theta_\mathrm{c})\,. \tag{6}$$

The importance of the selection function for cosmological studies lies in Eq. (3) which relates the cosmologically sensitive mass function to the observed catalog distribution. Accurate knowledge of Ψ is required in order to obtain constraints on cosmological parameters, such as the density parameter or the dark energy equation-of-state.

3. Simulations

Detailed study of SZ selection issues requires realistic simulations of proposed surveys. Although analytic arguments do provide significant insight, certain effects, such as cluster-cluster blending and confusion, can only be fully modeled with simulations. To this end, we have developed a rapid Monte Carlo-based simulation tool that allows us to generate a large number of realizations of a given survey. This is essential in order to obtain good measures of the selection function that are not limited by insufficient statistics. In this section we briefly outline our simulation method and our cluster detection algorithm, leaving details to Delabrouille et al. (2002) and Melin et al. (2004).

Unless explicitly stated, the simulations used in this work are for a flat concordance model (Spergel et al. 2003) with $\Omega_\mathrm{M} = 0.3 = 1 - \Omega_\Lambda$, Hubble constant of $H_0 = 70\ \mathrm{km\,s^{-1}\,Mpc^{-1}}$ Freedman et al. 2001) and a power spectrum normalization $\sigma_8 = 0.98$. The normalization of the $M - T$ relation is chosen to reproduce the local abundance of X-ray clusters with this value of σ_8 (Pierpaoli et al. 2001). Finally, we fix the gas mass fraction at $f_\mathrm{gas} = 0.12$ (e.g., Mohr et al. 1999).

3.1. Method

Our simulations produce sky maps at different frequencies and include galaxy clusters, primary CMB anisotropies, point sources and instrumental properties (beam smoothing and noise). In this work, we do not consider diffuse Galactic foregrounds, such as dust and synchrotron emission, as we are interested in more rudimentary factors influencing the selection function; we leave foreground issues to a future work (as general references, see Bouchet & Gispert 1999; Tegmark et al. 2000; Delabrouille et al. 2003).

We model the cluster population using the Jenkins et al. (2001) mass function and self-similar, isothermal β-profiles for the SZ emission. A realization of the linear density field $\delta\rho/\rho$ within a comoving 3D box, with the observer placed at one

end, is used to construct the cluster spatial distribution and velocity field. We scale the density field by the linear growth factor over a set of redshift slices (or bins) along the past light-cone of the observer; a set of mass bins is defined within each redshift slice. We then construct a random cluster catalog by drawing the number of clusters in each bin of mass and redshift according to a Poisson distribution with mean given by the mass function integrated over the bin. Within each redshift slice, we spatially distribute these clusters with a probability proportional to $1 + b\frac{\delta\rho}{\rho}$, where b is the linear bias given by Mo & White (1996). Comparison of the resulting spatial and velocity 2-point functions of the mock catalog with results from the VIRGO consortium's N-body simulations shows that this method faithfully reproduces the correlations down to scales of order of 10 h^{-1} Mpc.

Individual clusters are assigned a temperature using a $M - T$ relation consistent with the chosen value of σ_8 (Pierpaoli et al. 2001)

$$\frac{M}{10^{15}\, h^{-1}\, M_\odot} = \left(\frac{T}{\beta_p}\right)^{\frac{3}{2}} \left(\Delta_c E^2\right)^{-\frac{1}{2}} \tag{7}$$

with $\beta_p = 1.3 \pm 0.13 \pm 0.13$ keV. Here, Δ_c is the mean density contrast for virialization (weakly dependent on the cosmology) and $E(z) = H(z)/H_0$. As mentioned, we distribute the cluster gas with an isothermal β-model:

$$n_e(r) = n_e(0)\left[1 + \left(\frac{r}{r_c}\right)^2\right]^{\frac{-3\beta}{2}} \tag{8}$$

where we fix $\beta = 2/3$ and the core radius is taken to be $r_c = 0.1\, r_v$, with the virial radius given by

$$r_v = 1.69\, h^{-2/3} \left(\frac{M}{10^{15}\, M_\odot}\right)^{1/3} \left(\frac{\Delta_c}{178}\right)^{-1/3} E^{-2/3}\ \text{Mpc}. \tag{9}$$

The central electron density is determined by the gas mass fraction f_{gas}. For the present work, we ignore any intrinsic scatter in these scaling relations.

In this way we produce a 3×3 degree map of the SZ sky. Primary CMB anisotropies are added as a Gaussian random field by drawing Fourier modes according to a Gaussian distribution with zero mean and variance given by the power spectrum as calculated with CMBFAST (Seljak & Zaldarriaga 1996). We then populate the maps with radio and infrared point sources, using the counts summarized in Bennett et al. (2003) and fitted by Knox et al. (2003), and the counts from SCUBA (Borys et al. 2003). Finally, the map is smoothed with a Gaussian beam and white Gaussian noise is added to model instrumental effects.

3.2. Detection algorithm

We have developed (Melin et al. 2004) a rapid detection routine incorporating a deblending algorithm that is based on matched filtering (Haehnelt & Tegmark 1996), for single frequency surveys, and matched multi-filtering (Herranz et al. 2002), for multi-frequency surveys. Recall that in this work we only examine single frequency surveys. The matched filter, on a scale θ_c, is defined to yield the best linear estimate of the amplitude of the SZ signal from a cluster with (matched) core radius θ_c. It depends on both the beam-smoothed cluster profile τ_c and the noise power spectrum $P(k)$. In Fourier space it is given by

$$\hat{F}(\boldsymbol{k}) = \left[\int \frac{|\hat{\tau}_c(\boldsymbol{k}')|^2}{P(k')} \frac{d^2k'}{(2\pi)^2}\right]^{-1} \frac{\hat{\tau}_c^*(\boldsymbol{k})}{P(k)} \tag{10}$$

where $P = (P_{cmb} + P_{sources})|\hat{B}|^2 + P_{ins}$, $\hat{\tau}_c$ is the Fourier transform of the beam-smoothed cluster profile τ_c, $\hat{B}$ is that of the instrumental beam (a Gaussian), and P_{cmb}, $P_{sources}$ and P_{ins} represent the power spectra of the primary CMB anisotropies, residual point sources and instrumental noise, respectively. We denote the standard deviation of the noise (including primary CMB and residual points sources) passed through the filter at scale θ_c by σ_{θ_c}, and give its expression for future reference:

$$\sigma_{\theta_c} = \left[\int \frac{|\hat{\tau}_c(\boldsymbol{k})|^2}{P(k)} \frac{d^2k}{(2\pi)^2}\right]^{-\frac{1}{2}}. \tag{11}$$

This is the fluctuation amplitude of the filtered signal in the absence of any cluster signal.

We can summarize the detection algorithm in three steps:

- filter the observed map with matched filters on different scales θ_c in order to identify clusters of different sizes. This produces a set of filtered maps;
- in each filtered map, find the pixels that satisfy $\frac{S}{N} >$ *threshold* (e.g. 3 or 5). Define cluster candidates as local maxima among these pixels. At this point, each cluster candidate – in each map – has a position, size (that of the filter that produced the map), and a SZ flux given by the signal through the matched filter;
- identify cluster candidates across the different filtered maps using a tree structure (the same cluster can obviously be detected in several filtered maps) and eliminate multiple detections by keeping only cluster properties corresponding to the highest *S/N* map for each candidate.

4. Selection function for single frequency SZ surveys

We consider a single frequency SZ survey with characteristics representative of upcoming interferometers (e.g., the *Arcminute MicroKelvin Imager* being constructed in Cambridge[3]): a 15 GHz observation frequency, 2 arcmin *FWHM* (synthesized) beam and a noise level of 5 μK/beam. Note that, for simplicity and generality, we model the observations as a fully sampled sky map instead of actual visibilities. This approximation should be reasonably accurate given the good sampling expected in the Fourier plane; it will, however, miss important details of the selection function that will require adequate modeling when the time comes. In the same spirit, we also model the noise as a white Gaussian random variable with zero mean and the given variance.

During the course of the discussion, we will often compare the following observational cases: 1) no instrumental

[3] http://www.mrao.cam.ac.uk/telescopes/ami/index.html

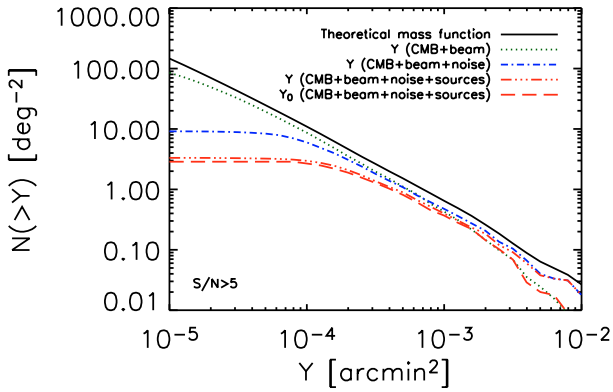

Fig. 1. Cluster counts in terms of integrated Y for the input concordance model (black solid line) and for detected clusters: the green dotted line gives the counts neglecting the effects of instrumental noise and point sources (CMB + beam = 2 arcmin *FWHM*); the blue dash-dotted line includes instrumental noise (5 μK/beam); the red dash-triple-dotted line further includes the effects of residual point sources after explicit subtraction of all sources with flux greater than 100 μJy (see text). These are all plotted as functions of the *true* total flux Y. The red dashed line shows the observed counts for the latter case in terms of the *observed* flux Y_o.

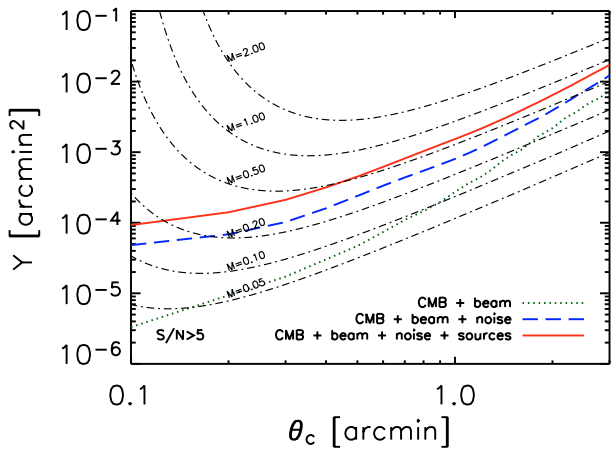

Fig. 2. Selection in the parameter plane of total flux Y and core radius θ_c. The three curves correspond to the different simulated cases, as indicated in the legend; all correspond to a cut at signal-to-noise of 5. The dot-dashed lines in the background give contours of constant mass in this plane; each is parameterized by redshift z. Note that cluster selection does not follow a simple flux cut, which would be a horizontal line, nor a simple mass cut. Photometric errors are neglected in this plot, meaning that observed cluster parameters Y_o and θ_c equal the true values Y and θ_c.

noise (CMB+beam[4]); 2) the former plus instrumental noise at 5 μK/beam; and 3) the previous plus point sources below a flux limit of 100 μJy at 15 GHz. In this last case, we are assuming that all sources brighter than the flux limit are explicitly subtracted; for example, both AMI and the SZA[5] plan long baseline observations for point source removal.

Integrated source counts in terms of total cluster flux Y (measured in arcmin^2) are shown in Fig. 1. The theoretical counts for the fiducial model are given by the solid black line, while the other curves give the counts from our simulated observations. They are plotted in terms of *true* flux Y, except for the red dashed curve that gives the counts as a function of *observed* flux Y_o, as would actually be observed in a survey. Differences between the detected cluster counts and the theoretical prediction (black solid line) reflect catalog incompleteness; the nature of this incompleteness is the focus of our discussion. The influence of photometric errors is illustrated by the difference between the observed counts as a function of observed flux (red dashed curve) and the detected-cluster counts given as a function of true flux.

4.1. Catalog completeness

It is important to understand the exact nature of the incompleteness evident in Fig. 1, and we shall now demonstrate that it is not simply a function of total flux. Our detection algorithm operates as a cut at fixed signal-to-noise, which leads to the following constraint on (true) cluster parameters Y and θ_c:

$$Y = y_{\rm est} \int {\rm d}\Omega\, \tau_c(\hat{n}) \geq \left(\frac{S}{N}\right) \sigma_{\theta_c} \int {\rm d}\Omega\, \tau_c(\hat{n}) \qquad (12)$$

[4] Note that in this case of no noise, the beam can be perfectly deconvolved.

[5] http://astro.uchicago.edu/sze

where $y_{\rm est}$ is the central Compton parameter estimated by the filter matched to a cluster of core radius θ_c, and the filter noise on this scale is given by Eq. (11). Figure 2 shows the resulting selection curves for our three cases in the $Y - \theta_c$ plane at $S/N \geq 5$. Note that we are speaking in terms of true cluster parameters, leaving the effects of photometric errors aside for the moment.

It is clear from this figure that cluster selection does not correspond to a simple flux cut – it depends rather on a combination of both source flux and angular extent. The exact form of this dependence is dictated by the noise power spectrum, which must be understood to include primary CMB anisotropy. That this latter dominates on the larger scales can be seen from the fact that the three curves approach each other at large core radii. For smaller objects, on the other hand, instrumental noise and residual point source contamination "pull" the curve towards higher fluxes relative to the ideal case that includes only CMB anisotropies (dotted line).

For the solid red curve, we calculate the flux variance induced by residual point sources at the given filter scale and then add the equivalent Gaussian noise term to the instrumental noise and CMB contributions. One may well ask why the source fluctuations should be Gaussian given the shallow slope of the radio source counts that would normally lead to very non-Gaussian statistics. The fluctuations are in fact Gaussian, as we have verified with the simulations, essentially because the source subtraction is performed at higher angular resolution than the smallest filter scale; in effect, we have cleaned "below" the filter confusion limit, so that the number of sources/filter beam is large and we approach the Gaussian limit. This realistically reflects what will actually be done with interferometers using long baseline observations for source subtraction.

The dot-dashed lines in the background of the figure represent contours of constant cluster mass $M(Y, \theta_c)$. They result

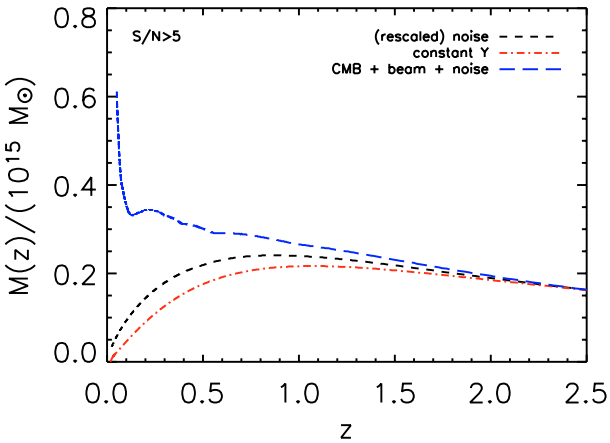

Fig. 3. Detection mass as a function of redshift. The blue long-dashed line shows the result for the case CMB + noise (blue long-dashed line in Fig. 2). The rise at low redshift is due confusion with primary CMB fluctuations that is more important for nearby clusters with large angular extent. The red dot-dashed line gives the result for a pure flux-limited catalog (see text), and the black short dashed line that for observations without CMB confusion (e.g., multi-frequency). Relative to a pure flux-limited catalog, both observed catalogs loose clusters over a range of redshifts.

from inversion of the $Y(M, z)$ and $\theta_c(M, z)$ relations, where we associate cluster core radius with filter scale. Note that redshift varies along each contour, and that we have assumed zero scatter in the relations so that the inversion is one-to-one. In reality, of course, they contain intrinsic scatter, due to cluster physics, as well as observational scatter induced by photometric errors. The position of these mass contours depends on both cluster physics and the underlying cosmology; we may, for example, displace the contours by changing the gas-mass fraction. The selection curves, in contrast, are independent of cosmology and cluster physics, being based on purely observational quantities.

Observed clusters populate this plane according to the distribution $\mathrm{d}N_o/\mathrm{d}Y_o\mathrm{d}\theta_{co}$, which depends on cluster physics, cosmology and photometry; Eq. (3) gives it in terms of the key theoretical quantity, the mass function. If photometric errors are assumed to be unimportant, then Eq. (6) applies and we see that the function $\chi(Y, \theta_c)$ is a step function taking the value of unity above the selection curves, and zero below; photometric errors simply "smooth" the selection function Φ as manifest by Eq. (5). Completeness expressed in terms of the function χ is therefore *independent* of cluster physics and cosmology. A more common way to express completeness is by the ratio of detected to actual clusters as a function of total flux (or angular scale). At a given flux, for example, this ratio is the fraction of clusters falling above the selection curve. Clearly, it depends on the distribution of clusters over the plane and is, hence, *dependent* on cluster physics, cosmology and photometry. We conclude that the function χ is a more useful description of a survey.

Figure 2 provides a concise and instructive view of cluster selection over the observational plane. We are of course ultimately interested in the kinds of objects that can be detected as a function of redshift, and to this end it is useful to study the *detection mass* shown in Fig. 3. This is defined as the smallest mass cluster detectable at each redshift given the detection criteria. For the figure, we assume that there is no scatter in the $Y_o(M, z)$ and $\theta_{co}(M, z)$ relations so that a selection curve in the observational plane uniquely defines the function $M_{\rm det}(z)$. Note that, as emphasized above, these detection mass curves depend on the assumed cosmology.

We compare three situations in the figure. The blue long-dashed line gives the detection mass for the case CMB + noise (single frequency experiment), while the red dot-dashed line shows the result for a pure flux-limited catalog. The chosen flux cut corresponds to the left-most point on the blue long-dashed selection curve in Fig. 2 (CMB+noise). Finally, the black short-dashed line gives the detection mass for a case with just instrumental noise (with the same beam as the previous cases) and no primary CMB; this approximates the situation for a multi-frequency experiment which eliminates CMB confusion. The noise level has been adjusted such that the selection curve in the (Y, θ_c)-plane matches the previous two cases on the smallest scales. With this choice, all three detection mass curves overlap at high z as seen in Fig. 3.

We see that that the observed catalog (blue long-dashed curve) looses clusters (i.e., has a higher detection mass) over a broad range of redshifts relative to the pure flux-limited catalog (red dot-dashed line); the effect is most severe for nearby objects, whose large angular size submerges them in the primary CMB anisotropies, but it remains significant out to redshifts of order unity. This is also reflected in the redshift distribution of Fig. 5 to be discussed below. We note in addition that even multi-frequency experiments loose clusters over a rather broad range of redshifts, as indicated by the difference between the lower two curves.

Simulations are needed to evaluate the importance of factors not easily incorporated into the simple analytic calculation of the cluster selection curve; these include source blending and morphology, other filtering during data analysis, etc. Using our simulations, we find that cluster detection in mock observations closely follows the analytic predictions, thus indicating that blending does not significantly change the above conclusions, at least for the case under study – a 2 arcmin beam with noise at a level of 5 μK/beam – representative of planned interferometer arrays. As our current simulations only employ spherical beta model profiles, they only test for the importance of blending effects; future work will include more realistic profiles taken, for example, from hydrodynamical N-body simulations. The simulations are also crucial for correctly evaluating the photometric precision of the survey catalog. Contrary to the situation for cluster detection, we find that blending greatly affects photometric measurements: photometric scatter from the simulations is significantly larger than expected based on the S/N ratio, whether the threshold is taken at $S/N = 5$ or 3.

4.2. Catalog contamination

Contamination by false detections is a separate function that can only be given in terms of observed flux and angular (or filter) scale; once again, simulations are crucial for evaluating effects such as blending and confusion. Figure 4 shows

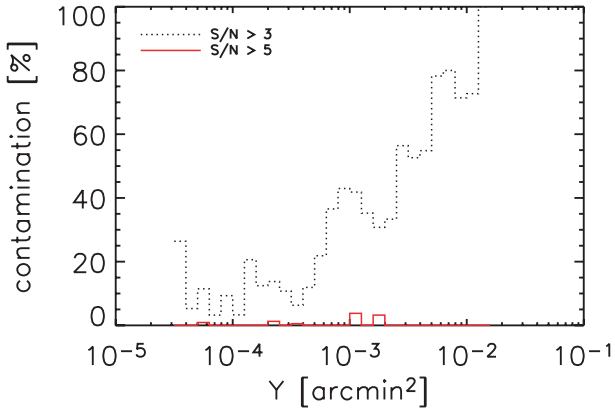

Fig. 4. Contamination rate for a single frequency survey as a function of total flux for two different detection thresholds. The histograms give the percentage of sources that are false detections in catalogs extracted from our simulations.

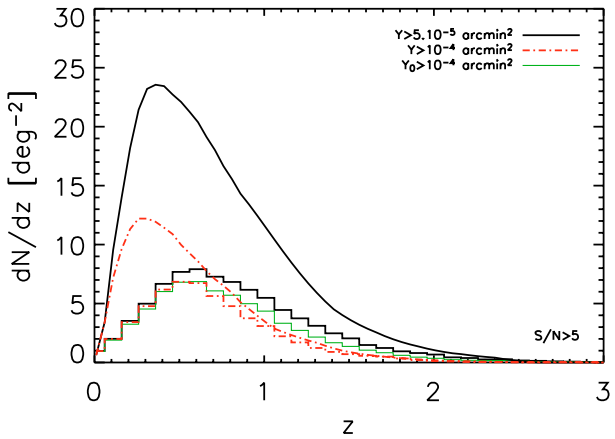

Fig. 5. Redshift distribution of SZ clusters (case 2 – without residual point source noise). The black solid and red dashed curves give the theoretically predicted counts at the two indicated flux limits. Corresponding distributions for the simulated recovered counts, with the same two flux cuts on the true Y, are shown by the black and red, dashed histograms; the small difference between the two reflects the flat observed counts in Fig. 1. The lighter, green histogram shows the simulated counts cut at an *observed* flux of $Y_o > 10^{-4}$ arcmin^2.

the contamination level in our extracted catalogs as a function of total flux Y. The level is significantly higher than expected from the *S/N* ratio, indicating that confusion and blending effects are clearly important. This is most obvious for the case with $S/N = 3$, where contamination rises towards the high flux end due to confusion with primary CMB fluctuations that are more prevalent on larger angular scales. Even at relatively low flux levels around 10^{-4} arcmin^2, we see that the contamination rate remains near or above 10% for the $S/N = 3$ case. This quantifies the the expectation that single frequency surveys will contend with a non-negligible level of contamination.

4.3. The redshift distribution

The example of extracting cosmological constraints from the redshift distribution of SZ detected clusters affords a good illustration of the importance of understanding the selection function. These constraints arise from the shape of the cluster redshift distribution, which is affected by such parameters as the matter density (Oukbir & Blanchard 1997) and the dark energy equation-of-state (Wang & Steinhardt 1998); this is in fact one of the primary motivations for performing SZ cluster surveys (Haiman et al. 2001). The important point is that the redshift distribution expected in a given cosmological model also depends on the catalog selection function. In the following discussion, we assume that the $Y(M, z)$ and $\theta_c(M, z)$ relations are perfectly known.

Consider the redshift distributions shown in Fig. 5 for an observation where residual point source contamination has been reduced to a negligible level (case 2). The black line represents the theoretical distribution for clusters with total flux $Y > 5 \times 10^{-5}$ arcmin^2, which corresponds to the point source detection limit on the smallest filter scale (leftmost point on the dashed blue curve in Fig. 2). This predicted distribution is very different from the actual distribution of clusters shown as the black histogram. It is clearly impossible to deduce the correct cosmological parameters by fitting a flux-limited theoretical curve to the observed distribution. This demonstrates that the point-source flux limit cannot be used to model the catalog redshift distribution, which is already clear from the fact that the counts in Fig. 1 have already turned over and the catalog is clearly incomplete.

One can try to cut the catalog at a higher flux limit of $Y > 10^{-4}$ arcmin^2, where the observed counts just begin to flatten out and incompleteness is not yet severe. Comparison of the dashed red line – theoretically predicted counts at this flux limit – with the red dashed histogram shows that the observed distribution still differs significantly from the predicted flux-limited redshift distribution. Modeling the observed catalog as a pure flux cut would again lead to incorrect cosmological constraints. In order to extract unbiased parameter estimates, one must adequately incorporate the full catalog selection criteria.

We may illustrate this point by considering the effect of an un-modeled CMB power excess at high l, such as suggested by the CBI experiment (Mason et al. 2001). As we have seen in Fig. 2, the primary CMB fluctuations influence the exact form of the selection curve in the (Y, θ_c) plane; their power on cluster scales must therefore be accurately known to correctly model the cluster selection function. The black curve and black histogram in Fig. 6 repeat the results of Fig. 5 for a cut at $Y > 5 \times 10^{-5}$ arcmin^2. In particular, the black histogram gives the redshift distribution of clusters extracted from simulations including a CMB power spectrum corresponding to the concordance model. The blue (lower) histogram shows the redshift distribution for clusters extracted from simulations in which additional CMB power has been added at high l – a constant power of $l(l+1)C_l/2\pi = 20\ \mu$K was smoothly joined to the concordance model CMB spectrum (just below $l = 2000$) and continuing out to $l = 3000$. Instead of plunging towards zero, as expected of the primary CMB fluctuations in the concordance model, this second model levels off at a constant power level on cluster scales. This has an important effect on cluster detection, as clearly evinced in the figure.

We now examine the effect of ignoring this excess power in an analysis aimed at constraining cosmological parameters.

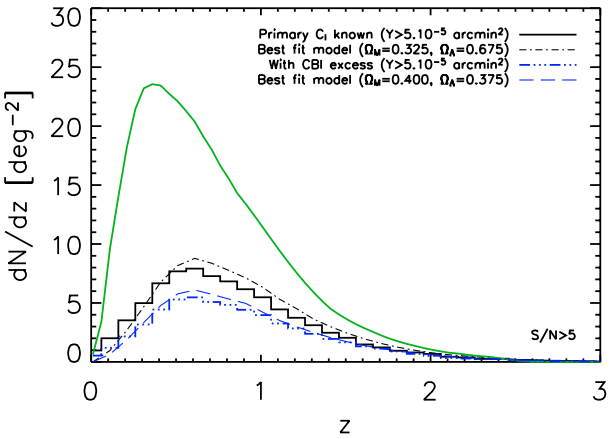

Fig. 6. Effect of incorrect modeling of the selection function. The black continuous curve and black (upper) histogram repeat the results of Fig. 5 for catalogs cut at a flux of $Y = 5 \times 10^{-5}$ arcmin^2 – the former for a pure flux-limited catalog, the latter for the clusters extracted from our concordance model simulations with the expected primary CMB power spectrum $[(\Omega_M, \Omega_\Lambda) = (0.3, 0.7)]$; note that the histogram is calculated as the average over 50 simulations of a 3×3 square degree survey field. The light black, dot-dashed curve is the best-fit model to the redshift distribution from a single such simulation; the constraints from for this fit are shown in Fig. 7. The lower (blue) histogram shows the distribution of clusters extracted from the same 50 simulations, but with excess primary CMB power added at high l (see text); once again, the histrogram is the average over the ensemble of simulations. The blue dashed curve shows the best-fit for the same realization as before – but now with the excess – *when ignoring the excess in the fitting* (incorrect selection function modeling). Corresponding constraints are shown in Fig. 7. Both fits are statistically acceptable (see text).

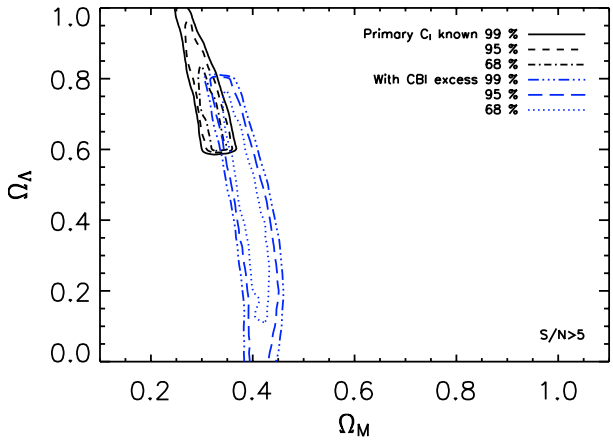

Fig. 7. Confidence contours for the fits discussed in Fig. 6, shown for a survey covering 3 × 3 sq. degrees. The upper (black) contours correspond to the case where the selection function is correctly modeled (no excess CMB power at high l); the best-fit parameters are $(\Omega_M, \Omega_\Lambda) = (0.325, 0.675)$ and 1σ contours fully enclose the true (simulation input) cosmological values of (0.3, 0.7). The larger (blue) contours represent the situation when the CMB excess is not properly accounted for by the selection function model. The best-fit parameter values are significantly biased – (0.4, 0.375) – and the true parameter values, lie outside the 99% contour. In both cases the fits are acceptable (see text).

This means that we ignore the excess both in the construction of the matched filter and in the selection function model needed for the fit. The former has only a relatively minor effect on the catalog extraction and observed histogram. The second effect is much more serious, as we now demonstrate.

Consider constraints on the parameter pair $(\Omega_M, \Omega_\Lambda)$ by fitting models to the redshift distribution of a 3 × 3 square degree survey. Note that the histograms shown in the figures are in fact averages taken over an ensemble of 50 such simulations, to avoid confusing statistical fluctuations. For the present example, however, we fit models to the redshift distribution from a single simulation. During the fit, we fix the Hubble parameter to its standard value ($H_0 = 70$ km s^{-1} Mpc^{-1}) and adjust the power spectrum normalization σ_8 to maintain the observed present-day cluster abundance (following Pierpaoli et al. 2001). For our simplified case of zero-scatter relations between (Y_o, θ_{co}) and (M, z), both the selection function Φ and the intrinsic scatter function T contain Dirac delta functions that collapse the various integrals in Eqs. (3) and (4). We then obtain the following expression for the redshift distribution of observed clusters brighter than a flux of Y_o:

$$\frac{dN_o}{dz}(>Y_o) = \int_{M(Y_o,z)}^{\infty} dM\, \chi\,[Y(M,z), \theta_c(M,z)]\, \frac{dN}{dz dM} \qquad (13)$$

where $M(Y, z)$ is the zero-scatter relation between flux and mass and redshift. All selection effects are encapsulated in the completeness function χ, whose dependence on the primary CMB power is the focus of our present discussion.

We consider two cases: the first with the expected concordance primary CMB power spectrum, the second with the CBI-like excess power. In the first case, we adopt the true power spectrum for catalog construction and modeling of χ – the selection function is properly modeled. In the second situation, we ignore the excess in both catalog construction and in fitting – the selection function is incorreclty modeled. When correctly modeling the selection function, we find best-fit values of $(\Omega_M, \Omega_\Lambda) = (0.325, 0.675)$. The light black dot-dashed curve in Fig. 6 shows that this model reasonably reproduces the predicted redshift distribution (black solid histogram), and the 1σ contours in Fig. 7 enclose the true (simulation input) values. The fit is good with a reduced $\chi^2 = 0.94$ (34 degrees-of-freedom). When incorrectly modeling the selection function, on the other hand, we find biased best-fit values of (0.4, 0.375), and, as shown in Fig. 7, the true parameter values fall outside the 99% confidence contours. Furthermore, this biased fit is acceptable with a reduced $\chi^2 = 1.17$ (31 degrees-of-freedom), giving no indication of its incorrectness. The redshift distribution of this model is shown as the light dashed (blue) curve in Fig. 6, faithfully reproducing the (averaged) histogram for this case. This is a particularly telling example of the importance of the selection function, because the primary CMB power on cluster scales is at present not well known. It will have to be constrained by the same experiments performing SZ cluster surveys; cosmological constraints will be correspondingly degraded, a subject we return to in a future work.

For another example of incorrect modeling of the selection function, consider that β and θ_c of real clusters may not behave as we assume when constructing the matched filter.

This will bias flux measurments and displace the selection curve in the (Y, θ_c) plane relative to our expectations, leading to an incorrect selection function model. As above, this will yield biased parameter estimates.

As a final note, and returning to Fig. 5, we show the distribution of detected clusters at the higher flux cut as a function of *observed* flux with the lighter, green histogram. The difference with respect to the corresponding distribution in terms of true flux (the red, dashed histogram) reflects statistical photometric errors; note that in fact this tends to falsely increase the number of objects seen at the higher redshifts. Although in this case photometric errors are of secondary importance to the observed redshift distribution (completeness effects dominate), they must also be fully accounted for in any cosmological analysis.

5. Discussion and conclusions

Our aim as been to emphasize the importance of understanding the SZ cluster selection function, as for any astronomical survey. We proposed a general definition of the selection function that can be used to directly relate theoretical cluster distributions to observed ones, and which has the nice property of clearly separating the influence of catalog incompleteness and photometric errors. It is a function of both observing conditions and of the detection and photometry algorithms used to construct the survey catalog. Defined over the (true) total flux-angular size plane, however, the selection function is independent of cosmology and cluster physics; its connection to theoretical cluster descriptors, such as mass and redshift, on the other hand, depends on both. A common way of quoting incompleteness in terms of total flux is similarly sensitive to cluster physics and underlying cosmology.

Using a matched spatial filter (Melin et al. 2004), we studied the selection function for single frequency SZ surveys, such as will be performed with upcoming interferometers[6]. Our main result is that a SZ catalog is not simply flux limited, and this has implications for cosmological studies. A simple analytic argument shows the exact manner in which catalog selection depends on both cluster flux and angular size; simulated observations indicate that this simple estimate is quite accurate and little affected by blending, although future work needs to take into account more realistic cluster profiles. We also noted that noise induced by residual point sources tends to be Gaussian, because subtraction of the brightest sources will be done at higher angular resolution than the smallest filter scale in the SZ maps.

The implications for cosmological studies were illustrated with the redshift distribution, which will serve to constrain cosmological parameters in future surveys. Theoretical redshift distributions based on a simple flux limit cannot fit observed distributions; at best they would lead to biased estimates of cosmological parameters. One must incorporate the complete selection criteria depending on both flux and angular extent, and hence have a good understanding of the catalog selection function. This understanding depends on a number of astrophysical factors in addition to instrumental parameters. Our example of an unmodeled primary CMB power excess (relative to the adopted concordance model) on small angular scales ($l \geq 2000$) highlights the point: we obtained biased parameter estimates because the selection function was incorrectly modeled; note that the false fit was in fact a good fit to the data, according to the χ^2. Other factors, for example, cluster morphology and its potential evolution, will also play a role. In the particular case of the CMB power excess, we note that accurate knowledge of the primary CMB power on cluster scales will come from the same experiments performing the cluster surveys. It will be necessary to constrain the primary CMB power at the same time as cluster extraction, a point we return to in a future work.

An issue currently receiving attention in the literature concerns SZ survey "calibration", by which is meant the empirical Establishment of the $Y(M, z)$ relation. This is clearly essential for any cosmological study. The fact that SZ catalog selection depends not only on total flux but also on angular size complicates the question of survey calibration, for it implies that one must additionally establish a $\theta_c(M, z)$ relation, or its equivalent with some other angular size measure. In fact, since the dispersion on Y and θ_c will in general be correlated, we need the full joint distribution for these observables as a function of mass and redshift. Photometric errors, which we find can be significant, further complicate the issue by increasing scatter in observed relations and hence making them more difficult to obtain.

Although in this work we have focused our detailed study on single frequency surveys, the general conclusions should carry over to multiple frequency observations. In closing we note that the selection function obviously has equally important implications for other studies based on SZ-detected cluster catalogs, such as spatial clustering, etc. For many of these studies, photometric errors, which we have only briefly touched on here, will take on even greater importance.

Acknowledgements. J.-B. Melin and J. G. Bartlett thank the France Berkeley Fund (grant "Precision Cosmology from CMB analysis") and the Lawrence Berkeley Laboratory for financial assistance and hospitality for a visit during which part of this work was completed. We also thank our anonymous referee for helpful and thoughfull comments.

References

Adami, C., Ulmer, M. P., Romer, A. K., et al. 2001, ApJS, 131, 391
Bahcall, N. A., Ostriker, J. P., Perlmutter, S., & Steinhardt, P. J. 1999, Science, 284, 1481
Barbosa, D., Bartlett, J. G., & Blanchard, A. 1996, A&A, 314, 13
Bartelmann, M. 2001, A&A, 370, 754
Bartlett, J. G. 2000 [arXiv:astro-ph/0001267]
Bartlett, J. G. 2001, Review in Tracing cosmic evolution with galaxy clusters, Sesto Pusteria 3–6 July 2001, ASP Conf. Ser., in press [arXiv:astro-ph/0111211]
Bennett, C. L., Hill, R. S., Hinshaw, G., et al. 2003, ApJS, 148, 97
Birkinshaw, M. 1999, Proc. 3K Cosmology, American Institute of Physics, Woodbury, 476, 298

[6] Although we have not here modeled the actual data taking in the visibility plane.

Borys, C., Chapman, S., Halpern, M., & Scott, D. 2003, MNRAS, 344, 385
Bouchet, F. R., & Gispert, R. 1999, New Astron., 4, 443
Carlstrom, J. E., Holder, G. P., & Reese, E. D. 2002, ARA&A, 40, 643
Delabrouille, J., Melin, J.-B., & Bartlett, J. G. 2002, in AMiBA 2001: High-Z Clusters, Missing Baryons, and CMB Polarization, ASP Conf. Proc. [arXiv:astro-ph/0109186]
Delabrouille, J., Cardoso, J.-F., & Patanchon, G. 2003, MNRAS, 346, 1089
Freedman, W. L., Madore, B. F., Gibson, B. K., et al. 2001, ApJ, 553, 47
Haehnelt, M. G., & Tegmark, M. 1996, MNRAS, 279, 545
Haiman, Z., Mohr, J. J., & Holder, G. 2001, ApJ, 553, 545
Herranz, D., Sanz, J. L., Hobson, M. P., et al. 2002, MNRAS, 336, 1057
Holder, G. P., Mohr, J. J., Carlstrom, J. E., Evrard, A. E., & Leitch, E. M. 2000, ApJ, 544, 629
Hu, W. 2003, Phys. Rev. D., 67, 081304
Jenkins, A., Frenk, C. S., White, S. D. M., et al. 2001, MNRAS, 321, 372
Jones, M. E., in AMiBA 2001: High-Z Clusters, Missing Baryons, and CMB Polarization, ASP Conf. Proc. [arXiv:astro-ph/0109351]
Kneissl, R., Jones, M. E., Saunders, R., et al. 2001, MNRAS, 328, 783
Knox, L., Holder, G. P., & Church, S. E. 2003 [arXiv:astro-ph/0309643]
Kosowsky, A. 2004 [arXiv:astro-ph/0402234]
Lima, M., & Hu, W. 2004 [arXiv:astro-ph/0401559]
Lo, K. Y., Chiueh, T. H., Martin, R. N., et al. 2000 [arXiv:astro-ph/0012282]
Majumdar, S., & Mohr, J. J. 2003 [arXiv:astro-ph/0305341]
Masi, S., Ade, P., de Bernardis, P., et al. 2003, Memorie della Societa Astronomica Italiana, 74, 96
Mason, B. S., Myers, S. T., & Readhead, A. C. S. 2001, ApJ, 555, L11
Melin, J.-B., et al. 2004, in preparation
Mo, H. J., & White, S. D. M. 1996, MNRAS, 282, 347
Mohr, J. J., Mathiesen, B., & Evrard, A. E. 1999, ApJ, 517, 627
Oukbir, J., & Blanchard, A. 1997, A&A, 317, 1
Peebles, P. J. E. 1993, Principles of Physical Cosmology, Princeton Series in Physics (New Jersey, Princeton: Princeton University Press)
Pierpaoli, E., Scott, D., & White, M. 2001, MNRAS, 325, 77
Rosati, P., Borgani, S., & Norman, C. 2002, ARA&A, 40, 539
Runyan, M. C., Ade, P. A. R., Bhatia, R. S., et al. 2003, ApJS, 149, 265
Schulz, A. E., & White, M. 2003, ApJ, 586, 723
Seljak, U., & Zaldarriaga, M. 1996, ApJ, 469, 437, www.cmbfast.org
Sunyaev, R. A., & Zel'dovich, Ya. B. 1970, Comments Astrophys. Space Phys., 2, 66
Sunyaev, R. A., & Zel'dovich, Ya. B. 1972, Comments Astrophys. Space Phys., 4, 173
Spergel, D. N., Verde, L., Peiris, H. V., et al. 2003, ApJS, 148, 175
Tegmark, M., Eisenstein, D. J., Hu, W., & Oliveira-Costa, A. 2000, ApJ, 530, 133
Wang, L., & Steinhardt, P. J. 1998, ApJ, 508, 483
White, M. 2003, ApJ, 597, 650

Web pages of various SZ experiments:

- ACBAR http://cosmology.berkeley.edu/group/swlh/acbar/
- ACT http://www.hep.upenn.edu/~angelica/act/act.html
- AMI http://www.mrao.cam.ac.uk/telescopes/ami/index.html
- AMiBA http://www.asiaa.sinica.edu.tw/amiba
- APEX http://bolo.berkeley.edu/apexsz
- BOLOCAM http://astro.caltech.edu/~lgg/bolocam_front.htm
- SPT http://astro.uchicago.edu/spt/
- SZA http://astro.uchicago.edu/sze
- Planck http://astro.estec.esa.nl/Planck/